

Anomalous Paramagnetic Effects in the Mixed State of $\text{LuNi}_2\text{B}_2\text{C}$

Tuson Park, A. Malinowski, M. F. Hundley, and J. D. Thompson
Los Alamos National Laboratory, Los Alamos, New Mexico 87545, USA

Y. Sun* and M. B. Salamon
*Department of Physics and Materials Research Laboratory,
University of Illinois at Urbana-Champaign, Urbana, Illinois 61801, USA*

Eun Mi Choi, Heon Jung Kim, and Sung-Ik Lee
*National Creative Research Initiative Center for Superconductivity and Department of Physics,
Pohang University of Science and Technology, Pohang 790-784, Republic of Korea*

P. C. Canfield and V. G. Kogan
Ames Laboratory, Department of Physics and Astronomy, Iowa State University, Ames, Iowa 50011, USA
(Dated: November 17, 2018)

Anomalous paramagnetic effects in dc magnetization were observed in the mixed state of $\text{LuNi}_2\text{B}_2\text{C}$, unlike any reported previously. It appears as a kink-like feature for $H \geq 30$ kOe and becomes more prominent with increasing field. A specific heat anomaly at the corresponding temperature suggests that the magnetization anomaly is due to a true bulk transition. A magnetic flux transition from a square to an hexagonal lattice is consistent with the anomaly.

In cuprate (high- T_c) superconductors, high-transition temperatures (T_c) and short coherence lengths (ξ) lead to large thermal fluctuation effects, opening a possibility for melting of the flux line lattice (FLL) at temperatures well below the superconducting transition temperature. A discontinuous step in dc magnetization and a sudden, kink-like drop in resistivity signified the first order nature of the melting transition from the vortex lattice into a liquid.^{1,2,3} In conventional type II superconductors, with modest transition temperatures and large coherence lengths, vortex melting is also expected to occur in a very limited part of the phase diagram,⁴ but it has yet to be observed experimentally. In the rare-earth nickel borocarbides $\text{RNi}_2\text{B}_2\text{C}$ ($R = \text{Y, Dy, Ho, Er, Tm, Lu}$), the coherence lengths ($\xi \cong 10^2 \text{ \AA}$) and superconducting transition temperatures (16.1 K for $R = \text{Lu}$) lie between these extremes, suggesting that the vortex melting will be observable and may provide further information on vortex dynamics. Indeed, Mun et al.⁵ reported the observation of vortex melting in $\text{YNi}_2\text{B}_2\text{C}$, based on a sharp, kink-like drop in electrical resistivity.

Recently, a magnetic field-driven FLL transition has been observed in the tetragonal borocarbides.^{6,7,8,9} The transition from square to hexagonal vortex lattice occurs due to the competition between sources of anisotropy and vortex-vortex interactions. The repulsive nature of the vortex interaction favors the hexagonal Abrikosov lattice, whose vortex spacing is larger than that of a square lattice. The competing anisotropy, which favors a square lattice, can be due to lattice effects (fourfold Fermi surface anisotropy),¹⁰ unconventional superconducting order parameter,¹¹ or an interplay of the two.^{12,13} In combination with non-negligible fluctuation effects, the competition leads to unique vortex dynamics right below the H_{c2} line in the borocarbides, namely a reentrant vor-

tex lattice transition.⁹ Fluctuation effects near the upper critical field line wash out the anisotropy effect, stabilizing the Abrikosov hexagonal lattice.^{14,15} Here, we report the first observation of paramagnetic effects in the dc magnetization M of the mixed state of $\text{LuNi}_2\text{B}_2\text{C}$. The kink-like feature in M and the corresponding specific heat feature for $H \geq 30$ kOe signify the reentrant FLL transition, which is consistent with the low-field FLL transition line inferred from small angle neutron scattering (SANS).⁹

Single crystals of $\text{LuNi}_2\text{B}_2\text{C}$ were grown in a Ni_2B flux as described elsewhere¹⁶ and were post-growth annealed at $T = 1000 \text{ C}^\circ$ for 100 hours under high vacuum, typically low 10^{-6} Torr.¹⁷ Samples subjected to a preparation process such as grinding, were annealed again at the same condition as the post-growth annealing. A Quantum Design magnetic property measurement system (MPMS) was used to measure ac and dc magnetization while the heat capacity option of a Quantum Design physical property measurement system (PPMS) was used for specific heat measurements. Electrical resistivity was measured by using a Linear Research ac resistance bridge (LR-700) in combination with a PPMS.

The detailed dc magnetization of $\text{LuNi}_2\text{B}_2\text{C}$ reveals an anomalous paramagnetic effect for $H \geq 30$ kOe, where the magnetic response deviates from a monotonic decrease and starts to rise, showing decreased diamagnetic response. The in-phase and out-of-phase components of the ac susceptibility χ_{ac} show a dip and the specific heat data show a feature at the corresponding temperature, reminiscent of vortex melting in high- T_c cuprates.¹⁸ Electrical transport measurements, however, do not exhibit any feature corresponding to the paramagnetic effect; *e.g.*, a sharp drop in the electrical resistivity. The zero-resistance transition, rather, occurs at a much higher temperature, suggesting that the paramag-

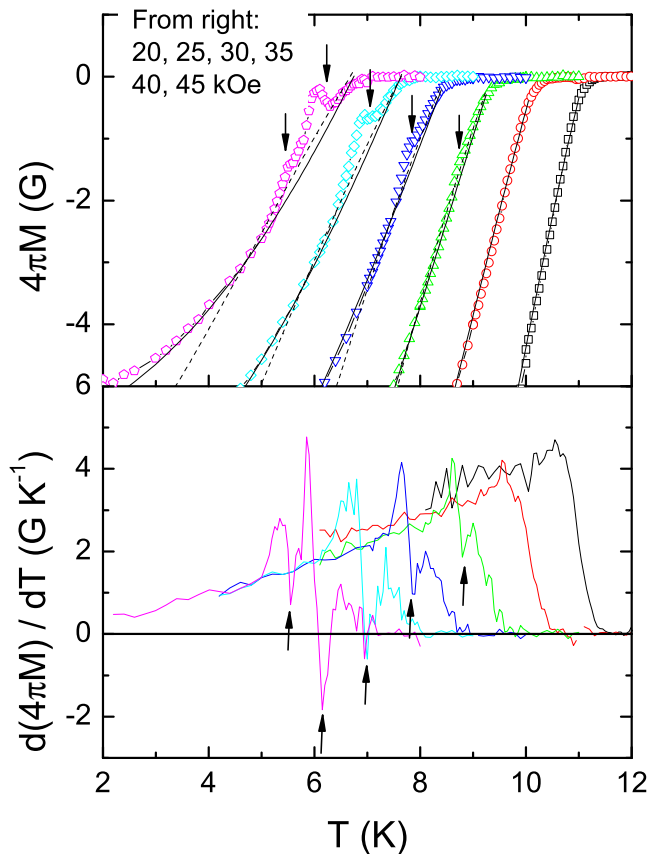


FIG. 1: (Color online). Top panel: dc magnetization $M(T)$ as a function of temperature at 20, 25, 30, 35, 40, and 45 kOe. Dashed lines are fits from the standard local London model¹⁹ and solid lines from the non-local London model¹⁴ (see text). Bottom panel: temperature derivation of $M(T)$ at corresponding magnetic fields. Arrows indicate the points where kink-like features start to appear

netic effect is not related to vortex melting. It is instead consistent with a topological FLL change between square and hexagonal structures.

The top panel of Fig. 1 shows dc magnetization M as a function of temperature at several fields. For $H \geq 30$ kOe, kink-like features appear, which are marked by arrows. The anomalous increase can be easily seen as a sharp drop in dM/dT (arrows in the bottom panel). The magnetization reported here is independent of time and has no hysteresis between zero-field cool (ZFC) and field cool (FC) data within experimental accuracy, indicating that the measured value is an equilibrium magnetization. In the top panel of Fig. 1, we compare the data and some model calculations. Dashed lines are predictions from the standard local London model:¹⁹

$$-4\pi M = M_0 \ln(\eta H_{c2}/H), \quad (1)$$

where $M_0 = \phi_0/8\pi\lambda^2$, η is a constant of order unity, λ the penetration depth, and ϕ_0 the flux quantum. In the fit, H_{c2} was determined from our resistivity data (see Fig. 2) and M_0 from H_{c2} with $\kappa = \lambda/\xi = 15$. In or-

der to get the best result, the fitting parameter η was varied between 0.95 and 0.97 and the absolute amplitude of M_0 was changed as a function of magnetic field. The local London model explains the monotonic decrease with decreasing temperature, but the fit becomes worse at higher field. In a clean system like $\text{LuNi}_2\text{B}_2\text{C}$ where the electronic mean free path is long compared to the coherence length ξ_0 , the current at a point depends on magnetic fields within a characteristic length ρ , or nonlocal radius. Taking into account the nonlocal current-field relation in superconductors, a non-local London model was suggested:²⁰

$$-4\pi M = M_0[\ln(1 + H_0/H) - H_0/(H_0 + H) + \Lambda], \quad (2)$$

where $H_0 = \phi_0/(4\pi^2\rho^2)$ and $\Lambda = \eta_1 - \ln(1 + H_0/\eta_2 H_{c2})$ with η_1 and η_2 being order of unity. It is worth noting that the scaling parameter H_{c2} in the local theory is replaced by H_0 in the non-local model. The nonlocal radius ρ slowly decreases with increasing temperature and is suppressed strongly by scattering. The solid lines are best results from the model calculation where we used the temperature dependence of H_0 and Λ from the literature for $\text{YNi}_2\text{B}_2\text{C}$.²¹ Both the local and the non-local models explain the temperature dependence of M at low fields, while only the non-local model can describe the data at and above 35 kOe. The good fit from the nonlocal model is consistent with the equilibrium magnetization analysis of $\text{YNi}_2\text{B}_2\text{C}$,²¹ suggesting the importance of nonlocal effects in the magnetization. The many fitting parameters in both fits, however, prevent us from making a definite conclusion as to which model better describes $M(T)$. Nevertheless, we can extract the important conclusion that the kink-like feature in the mixed state is a new phenomenon that needs further explanation.

In the early stage of high- T_c cuprate research, anomalous paramagnetic effects in $M(T)$ were reported in the irreversible region and this effect was later attributed to the field inhomogeneity of the measured scan length in a SQUID magnetometer.²² We tested various scan lengths from 1.8 cm to 6 cm for which the field inhomogeneity varies from 0.005 % to 1.4 % along the scan length and found negligible dependence on the measuring length, which suggests that field inhomogeneity is not the source of the anomaly. A more definitive test used a conventional type II superconductor NbSe_2 in a similar configuration. There was no such anomalies in NbSe_2 as in the borocarbide. Taken together, we conclude that the reversible paramagnetic effects are intrinsic to $\text{LuNi}_2\text{B}_2\text{C}$. We also emphasize that the phenomena is different from the paramagnetic Meissner effect (PME) or Wohlleben effect²³ where the FC χ becomes positive whereas the ZFC χ remains negative. The PME is an irreversible effect and occurs in the Meissner state, while the subject of this study is a reversible effect and takes place in the mixed state.

In the top panel of Fig. 2 the reversible magnetization M (left axis) and the out-of-phase component of ac susceptibility χ''_{ac} (right axis) are shown as a function of

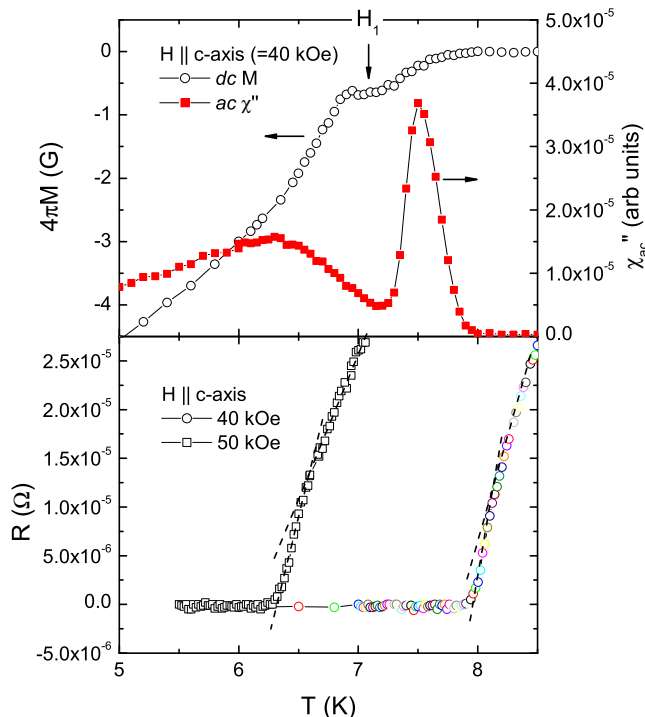


FIG. 2: (Color online). Top panel: Magnetization (left axis) and the imaginary part of the ac susceptibility (right axis) at 40 kOe. Bottom panel: Resistive superconducting transition at 40 kOe (circles) and 50 kOe (squares). The lines are guide to eyes.

temperature at 40 kOe. A dip appears both in χ'_{ac} (not shown) and in χ''_{ac} at the same temperature where M shows the paramagnetic anomaly. Since a dip in χ_{ac} is often related to vortex melting, it is natural to consider the vortex phase change from liquid to lattice or glass as a possible explanation. The resistive superconducting transition at 40 kOe (circles) and 50 kOe (squares) are shown in the bottom panel of Fig. 2. A resistive slope change in the transition region, that can be considered as a signature of the vortex melting,⁵ was observed at 8.1 K and 6.6 K for 40 kOe and 50 kOe, respectively. The $R = 0$ transition temperature, however, is much higher than the temperature where the dip occurs in χ_{ac} , which argues against the vortex melting scenario as the physical origin of the anomalous paramagnetic effects. The increase in M at the transition temperature is also opposite from the decrease in the vortex melting interpretation.

Recently, a structural phase transition in the FLL was suggested to explain another peak effect observed below the vortex melting line in YBCO.^{24,25} The vanishing of a *squash* elastic mode gives rise to a topological FLL transition and leads to the new peak effect, while the softening of the shear modes c_{66} is relevant to the conventional peak effect in high- T_c cuprates.²⁶ The observation of the dip effect well below the melting line in $\text{LuNi}_2\text{B}_2\text{C}$ indicates that the anomalous paramagnetic effects are related to a change in the FLL and

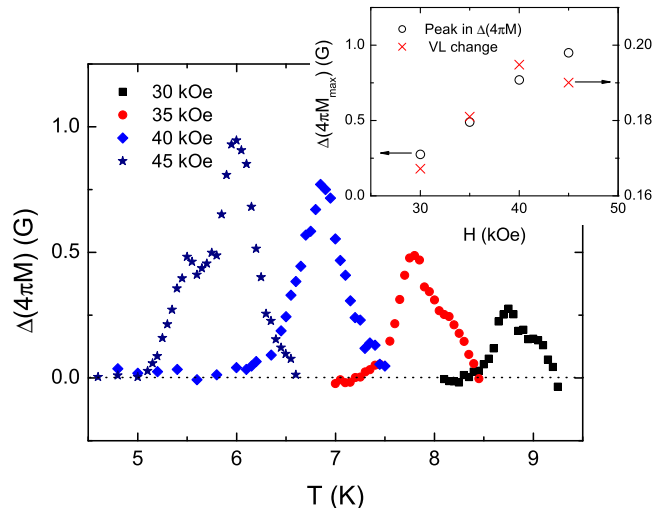


FIG. 3: (Color online). Temperature dependence of $\Delta(4\pi M)$ at 30, 35, 40, and 45 kOe, where $\Delta M = M - M(\text{nonlocal})$. Inset: The peak values of $\Delta(4\pi M)$ are compared with those estimated from Eq. (3).

the increase in M is also consistent with the FLL change where the Abrikosov geometrical factor β changes.^{19,27} Fig. 3 shows the temperature dependence of the paramagnetic anomaly, $\Delta(4\pi M)$, at several magnetic fields, where $\Delta(4\pi M)$ is the magnetization after subtracting the monotonic, diamagnetic background obtained from Eq. (2). With increasing field, the peak becomes enhanced and an additional peak is observed at 45 kOe. In extreme type II material ($\kappa \gg 1/\sqrt{2}$), the magnetization change due to a FLL transition is written as

$$\Delta(4\pi M) = \frac{H_{c2} - H}{2\kappa^2 - 1} \left(\frac{1}{\beta_\Delta} - \frac{1}{\beta_\phi} \right), \quad (3)$$

where $\beta_\Delta \approx 1.16$ for a hexagonal FLL and $\beta_\phi \approx 1.18$ for a square FLL.¹⁹ In the inset of Fig. 3, we compared the peak intensity of $\Delta(4\pi M)$ (left axis) and the estimation from Eq. 3 (right axis) with $\kappa = 15$. It is encouraging to see that the simple model qualitatively reproduces the field dependence of the paramagnetic contribution. However, the quantitative difference in absolute values suggests that a more elaborate model is required.

The $H - T$ phase diagram is shown in Fig. 4. The upper critical field line H_{c2} was determined from the $R = 0$ superconducting transition and is consistent with the temperature where χ_{ac} starts to have a non-zero value. The H_1 line in the mixed state is the point where the reversible magnetization shows the paramagnetic effects and H_2 is the 2nd anomaly that appears above 45 kOe (see Fig. 1). According to the Gurevich-Kogan non-local London model,¹⁴ the anisotropic nonlocal potential, which is responsible for the low-field FLL transition observed in SANS,⁹ is averaged out by thermal vortex fluctuations near H_{c2} . Since the interaction becomes isotropic, the hexagonal Abrikosov lattice is preferable, leading to the second FLL transition from square back

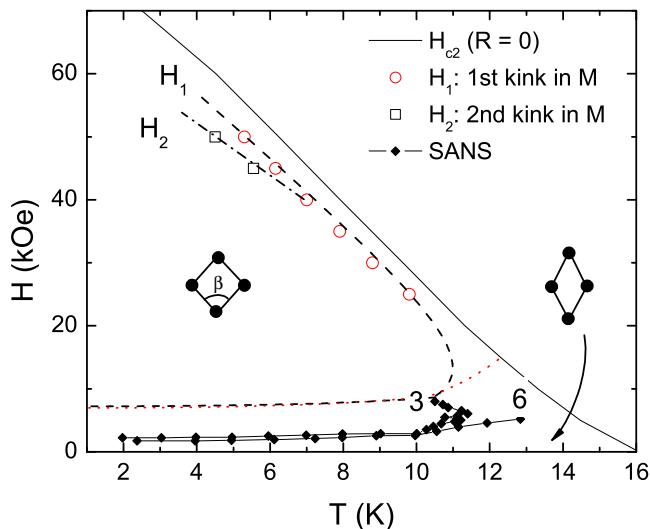


FIG. 4: (Color online). $H - T$ phase diagram. The H_1 line indicates the temperature where $M(T)$ deviates from a monotonic decrease and the H_2 line is where the second anomaly occurs above 45 kOe. The dashed line depicts qualitatively what fluctuation models based on the nonlocal London¹⁴ or extended GL¹⁵ predict when the nonlocal radius is approximately $2 - 3 \xi_0$. The dotted line is from theories without fluctuation effects.^{28,29} The diamonds are SANS data, where the numbers next to the data indicate the degrees of the azimuthal splitting with which the transition line is determined.⁹ The square and rhombic shapes are forms of vortex lattices.

to rhombic (triangular) lattice as the field gets closer to the H_{c2} line. The reentrant transition is predicted to occur well below the vortex melting line because the amplitude of vortex fluctuations required to wash out the nonlocal effects is much smaller than that for the vortex melting. This prediction is consistent with our observation that the H_1 line is much below the $R = 0$ transition line. The dashed line depicts qualitatively what the fluctuations models based on the nonlocal London¹⁴ or extended GL¹⁵ predict, which nicely explains the H_1 line. The dotted line is the FLL transition line that meets the H_{c2} line both in the non-local London model²⁸ and in the extended Ginzburg-Landau (GL) theory²⁹ without fluctuation effects. We note that a direct comparison between the SANS and our data is difficult even though they are qualitatively similar. Since H_1 heavily depends on the sample purity,³⁰ a factor of 2 or more difference in H_1 has been easily observed even among pure compounds.^{31,32} Further, the H_1 line from the SANS also depends on the criteria used for the FLL transition (see Fig. 4).

For vortex melting, where the lattice changes to a liquid, the transition involves latent heat and the specific heat shows a sharp peak at the transition temperature.¹⁸ For a structural change in the vortex lattice, the transition is probably of 2nd order because an infinitesimally small change of the angle β between adjacent vortex lines changes the symmetry. Based on the paramagnetic jump

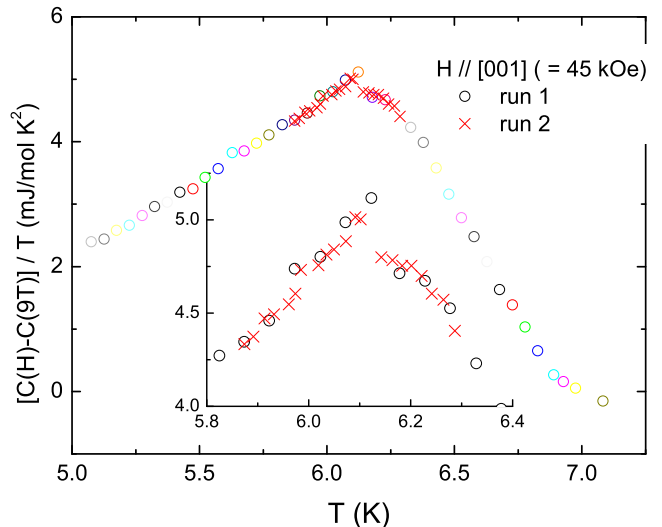


FIG. 5: (Color online). Specific heat difference $C(H)/T - C(9T)/T$ vs T at 45 kOe for $H \parallel [001]$. Inset: blow-up of the main panel at around 6.1 K. Different symbols correspond to different sets of measurements and attest to the reproducibility of these results.

(Fig. 1) and $dH_1/dT < 0$ (Fig. 3), Ehrenfest's relation at constant field predicts a suppression of C/T as the FLL changes from a rhombic to a square lattice. Fig. 5 shows the specific heat data of $\text{LuNi}_2\text{B}_2\text{C}$ at 45 kOe as a function of temperature. In addition to the superconducting transition between 6.22 and 6.89 K, an anomaly is, indeed, observed at 6.12 K which corresponds to the anomalous paramagnetic effects. Depending on the background we choose, however, the anomaly can be considered as either a suppression or a jump.³³ Similar features at 40 and 50 kOe were also observed at the temperatures corresponding to the paramagnetic effects in H_1 . More sensitive measurements such as ac calorimetry will help in resolving the issue. Finally, we note that we are not able to discern any corresponding feature to the H_2 line in C_p or in χ_{ac} . More work is in progress to understand the second paramagnetic jump in M which appears for $H \geq 45$ kOe.

In summary, we report the first observation of an anomalous paramagnetic jump in the magnetization of the mixed state of $\text{LuNi}_2\text{B}_2\text{C}$. A dip appears in χ_{ac} at the same temperature as the paramagnetic effects, suggesting the relevance of the flux line lattice. The $H - T$ phase diagram is consistent with a FLL structural transition from square to hexagonal lattice just below the upper critical field line. The observation of an additional feature in the specific heat data at the corresponding temperature underscores the interpretation of paramagnetic effects as due to a reentrant FLL transition in $\text{LuNi}_2\text{B}_2\text{C}$.

Work at Los Alamos was performed under the auspices of the U.S. Department of Energy (DOE) and at Urbana under NSF Grant No. DMR 99-72087. The work at Pohang was supported by the Ministry of Science and

Technology of Korea through the Creative Research Initiative Program and at Ames by Iowa State University of Science and Technology under DOE Contract No. W-

7405-ENG-82. We acknowledge benefits from discussion with Lev N. Bulaevskii, M. P. Maley, and I. Vekhter. We thank T. Darling for assistance in sample annealing.

-
- * Current address: Institute of Physics Chinese Academy of Sciences, Beijing 100080, People's Republic of China
- ¹ H. Pastoriza, M. F. Goffman, A. Arribere, and F. de la Cruz, *Phys. Rev. Lett.* **72**, 2951 (1994).
 - ² E. Zeldov, D. Majer, M. Konczykowski, V. B. Geshkenbein, V. M. Vinokur, and H. Shtrikman, *Nature (London)* **375**, 373 (1995).
 - ³ U. Welp, J. A. Fendrich, W. K. Kwok, G. W. Crabtree, and B. W. Veal, *Phys. Rev. Lett.* **76**, 4809 (1996).
 - ⁴ G. Eilenberger, *Phys. Rev.* **164**, 628 (1967).
 - ⁵ M.-O. Mun, S.-I. Lee, W. C. Lee, P. C. Canfield, B. K. Cho, and D. C. Johnston, *Phys. Rev. Lett.* **76**, 2790 (1996).
 - ⁶ U. Yaron, P. Gammel, D. Huse, R. Kleiman, C. Oglesby, E. Bucher, B. Batlogg, D. Bishop, K. Mortensen, and K. Clausen, *Nature (London)* **382**, 236 (1996).
 - ⁷ M. R. Eskildsen, K. Harada, P. L. Gammel, A. B. Abrahamsen, N. H. Andersen, G. Ernst, A. P. Ramirez, D. J. Bishop, K. Mortensen, D. G. Naugle, et al., *Nature (London)* **393**, 242 (1998).
 - ⁸ H. Sakata, M. Oosawa, K. Matsuba, N. Nishida, H. Takeya, and K. Hirata, *Phys. Rev. Lett.* **84**, 1583 (2000).
 - ⁹ M. R. Eskildsen, A. B. Abrahamsen, V. G. Kogan, P. L. Gammel, K. Mortensen, N. H. Andersen, and P. C. Canfield, *Phys. Rev. Lett.* **86**, 5148 (2001).
 - ¹⁰ V. G. Kogan, M. Bullock, B. Harmon, P. Miranovic, L. Dobrosavljevic-Grujic, P. L. Gammel, and D. J. Bishop, *Phys. Rev. B* **55**, R8693 (1997).
 - ¹¹ R. Gilardi, J. Mesot, A. Drew, U. Divakar, S. L. Lee, E. M. Forgan, O. Zaharko, K. Conder, V. K. Aswal, C. D. Dewhurst, et al., *Phys. Rev. Lett.* **88**, 217003 (2002).
 - ¹² N. Nakai, P. Miranovic, M. Ichioka, and K. Machida, *Phys. Rev. Lett.* **89**, 237004 (2002).
 - ¹³ T. Park, E. E. M. Chia, M. B. Salamon, E. D. Bauer, I. Vekhter, J. D. Thompson, E. M. Choi, H. J. Kim, S.-I. Lee, and P. C. Canfield (2004), unpublished.
 - ¹⁴ A. Gurevich and V. G. Kogan, *Phys. Rev. Lett.* **87**, 177009 (2001).
 - ¹⁵ A. D. Klironomos and A. T. Dorsey, *Phys. Rev. Lett.* **91**, 097002 (2003).
 - ¹⁶ B. K. Cho, P. C. Canfield, L. L. Miller, D. C. Johnston, W. P. Beyermann, and A. Yatskar, *Phys. Rev. B* **52**, 3684 (1995).
 - ¹⁷ X. Y. Miao, S. L. Bud'ko, and P. C. Canfield, *J. Alloys Comp.* **338**, 13 (2002).
 - ¹⁸ A. Schilling, R. A. Fisher, N. E. Phillips, U. Welp, W. K. Kwok, and G. W. Crabtree, *Phys. Rev. Lett.* **78**, 4833 (1997).
 - ¹⁹ P. G. deGennes, *Superconductivity of Metals and Alloys* (Benjamin, New York, 1966).
 - ²⁰ V. G. Kogan, A. Gurevich, J. H. Cho, D. C. Johnston, M. Xu, J. R. Thompson, and A. Martynovich, *Phys. Rev. B* **54**, 12386 (1996).
 - ²¹ K. J. Song, J. R. Thompson, M. Yethiraj, D. K. Christen, C. V. Tomy, and D. M. Paul, *Phys. Rev. B* **59**, R6620 (1999).
 - ²² A. Schilling, H. R. Ott, and T. Wolf, *Phys. Rev. B* **46**, 14253 (1992).
 - ²³ W. Braunsch, N. Knauf, G. Bauer, A. Kock, A. Becker, B. Freitag, A. Grutz, V. Kataev, S. Neuhausen, B. Roden, et al., *Phys. Rev. B* **48**, 4030 (1993).
 - ²⁴ K. Deligiannis, P. A. J. deGroot, M. Oussena, S. Pinfeld, R. Langan, R. Gagnon, and L. Taillefer, *Phys. Rev. Lett.* **79**, 2121 (1997).
 - ²⁵ B. Rosenstein and A. Knigavko, *Phys. Rev. Lett.* **83**, 844 (1999).
 - ²⁶ A. I. Larkin, M. C. Marchetti, and V. M. Vinokur, *Phys. Rev. Lett.* **75**, 2992 (1995).
 - ²⁷ A. A. Abrikosov, *Sov. Phys. JETP* **5**, 1174 (1957).
 - ²⁸ I. Affleck, M. Franz, and M. H. S. Amin, *Phys. Rev. B* **55**, R704 (1997).
 - ²⁹ Y. DeWilde, M. Iavarone, U. Welp, V. Metlushko, A. E. Koshelev, I. Aranson, G. W. Crabtree, and P. C. Canfield, *Phys. Rev. Lett.* **78**, 4273 (1997).
 - ³⁰ P. L. Gammel, D. J. Bishop, M. R. Eskildsen, K. Mortensen, N. H. Andersen, I. R. Fisher, K. O. Cheon, P. C. Canfield, and V. G. Kogan, *Phys. Rev. Lett.* **82**, 4082 (1999).
 - ³¹ M. R. Eskildsen, P. L. Gammel, B. P. Barber, A. P. Ramirez, D. J. Bishop, N. H. Andersen, K. Mortensen, C. A. Bolle, C. M. Lieber, and P. C. Canfield, *Phys. Rev. Lett.* **79**, 487 (1997).
 - ³² M. R. Eskildsen, A. B. Abrahamsen, D. Lopez, P. L. Gammel, D. J. Bishop, N. H. Andersen, K. Mortensen, and P. C. Canfield, *Phys. Rev. Lett.* **86**, 320 (2001).
 - ³³ When we extrapolate the specific heat data from above the H1 transition temperature (= 6.15 K) and consider them as a background, the feature at H1 can be considered as a decrease.